Eur. Phys. J. B **37**, 499–506 (2004)
DOI: 10.1140/epjb/e2004-00086-0

THE EUROPEAN PHYSICAL JOURNAL B

# Effect of pinning fields on the spin wave band gaps in comblike structures

H. Al-Wahsh[1], A. Akjouj[2,a], B. Djafari-Rouhani[2], A. Mir[3], and L. Dobrzynski[2]

[1] Faculty of Engineering, Zagazig University, Benha Branch, 11241 Cairo, Egypt
[2] Laboratoire de Dynamique et Structures des Matériaux Moléculaires, ESA CNRS 8024, UFR de Physique, Université de Lille1, 59655 Villeneuve d'Ascq Cedex, France
[3] Département de Physique, Faculté des Sciences, Université Moulay Ismail, Meknès, Morocco

Received 15 May 2003 / Received in final form 17 October 2003
Published online 9 April 2004 – 

**Abstract.** We consider, in the frame of the long-wavelength Heisenberg model, the effect of a pinning field on the spin wave band gaps and transmission spectra of one-dimensional comb-like structures. Using a Green's function method, we obtained closed-form expressions for the band structure and the transmission coefficients for an arbitrary value of the number $N$ of sites ($N'$of resonators) in the comb-like structure. We report the opening-up of stop bands inside the pass-bands due to the effect of the pinning field at the ends of the resonators of the comb. These structures, composed of one-dimensional ferromagnetic materials, may exhibit large gaps where the propagation of spin waves is forbidden. The width and frequency position of these gaps depends on the strength of the pinning field.

**PACS.** 75.30.Gw Magnetic anisotropy – 75.30.Ds Spin waves – 75.75.+a Magnetic properties of nanostructures

## 1 Introduction

In recent years, a great deal of interest has been devoted to the investigation of low-dimensional magnetic structures [1–3]. This related both to the fundamental interest and to the potential applications of spintronic devices, and is supported by the advanced progress in nanofabrication technology [4]. For example, arrays of very long ferromagnetic nanowires of Ni, permalloy and Co, with diameters in the range of 30 to 500 nm have been created [5,6]. These are very uniform in cross section, with lengths in the range of 20 microns. They thus are realizations of nanowires one can reasonably view as infinite in length, to excellent approximation. Besides the static and magneto-transport properties of magnetic nanowire arrays, the dynamic properties of magnetic nanostructure are also of considerable interest in both fundamental as well as applied research [6]. The static properties of micron-size magnetic dots and wires have been studied to some extent [7–10], while their high-frequency dynamic properties have been rarely investigated [11,12]. The study of spin waves is a powerful method for probing the dynamic properties of magnetic media in general and those of laterally patterned magnetic structures in particular [13]. On the other hand, due to the possible use of electron spin for storage and information transfer in quantum computers [14], there have been many recent studies on spin transport in semiconductor nanostructures [15]. In the last decade, several studies have addressed the problem of spin wave band structures in magnetic superlattices [16–19] and two-dimensional (2D) magnetic periodic structures [20]. Most of these studies focus on the existence of stop bands in the spin wave spectra of magnetic structures. These recent developments encouraged us to investigate magnetic excitations in networks composed of one dimensional (1D) continuous magnetic media. Our choice of 1D magnetic structures is motivated by possible engineer spin-injection devices that render feasible the control of the widths of the pass-bands (and hence the stop bands).

In previous publication, we proposed [21] a model of 1D structure exhibiting pass bands separated by large stop bands. The geometry of the model (Fig. 1a) (called *a comb-like structure* CLS) is composed of an infinite 1D monomode waveguide (*the backbone*, medium 1) along which $N'$ side branches of length $d_2$ (medium 2) are grafted at $N$ equidistant sites separated by a length $d_1$, $N$ and $N'$ being integers. The presence of defect branches in the comb structure can give rise to localized states within the gaps. It has been shown that these states are very sensitive to the length and number of the side

[a] e-mail: abdellatif.akjouj@univ-lille1.fr

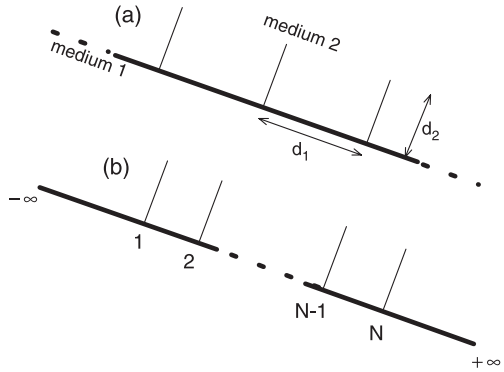


**Fig. 1.** (a) Schematic of the comblike waveguide investigated in the present work. The material media are designated by an index $i$, with $i$ equal 1 for the backbone (heavy line) and 2 for the side branches. There are $N'(=1)$ side branches of length $d_2$ grafted at equidistant sites separated by a length $d_1$. (b) Waveguide with $N'(=1)$ side branches of length $d_2$ grafted at a finite number $N$ of equidistant sites separated by a length $d_1$ and connected at its extremities to two semi-infinite leading lines.

branches, to the periodicity of the system, and to the length of the defect branches.

Let us direct attention to the point that the quantum size effect (or the sub-band structure) was neglected in the CLS networked waveguide. We dealt with a magnetic network where the cross-sections of all wires are considered to be much smaller than the considered wavelength, i.e. a continuum approximation theory was employed in the calculation. Such an approximation is valid provided that the relevant wavelengths are large compared with the lattice spacing, i.e. we dealt only with long-wavelength excitations. Therefore, in using the Heisenberg model of a ferromagnet we are neglecting the dipole-dipole interactions compared with the exchange contribution to the Hamiltonian [21,22]. This macroscopic approach is analogous to that used by Cottam [23] in magnetostatic calculations. Let us mention also that the continuum theory has the advantages that explicit analytic expressions of different magnetic properties (e.g. dispersion curves, transmission coefficients) can be calculated.

The purpose of the present note is to explore the effect of the pinning field [22] (acting at the end of the resonators of the CLS) on the spin waves band gaps and transmission spectra of a simple Heisenberg ferromagnet. We focus our attention on the effect of the pinning field because they can vary over a wide range of values, depending on the nature of the ends of the resonators and the properties of the magnetic bearing ions. If one has a perfect semi-infinite ferromagnetic medium (wire), in which the surface layer (end) has the same atomic structure and lattice constant as a similar crystallographic plane in the interior of the medium, then the crystal field at a site in the surface layer will have a lower symmetry than the crystal field at an interior site. This fact, combined with the presence of spin-orbit coupling can give rise to pinning fields in the surface layer [24]. While one might expect this contribution to the pinning field to be small if the magnetic ion is an S-state, if orbital degeneracy is present, one may expect rather strong surface pinning field to be generated even in a crystallographically perfect surface.

It is clear, as mentioned above, that one can encounter effective pinning field that vary in magnitude over a wide range. Since a pinning field at the ends of the resonators can strongly affect the spin motion near the boundary, therefore the spin waves frequencies can be severely modified. We shall examine this effect for a wide range of pinning field in this work. Such an effect may lead to new features, in comparison with the CLS waveguides studied in reference [21]. For example, the existence of larger gaps, the avoidance of the constraint on the boundary condition at the end of the side branches, appearance of quasi quantized bands (at large pinning) without inserting a defect. Theses new features (which could be of potential interest in waveguide structures) are essentially due to the influence of the pinning field at the end of the resonators. We report on results of calculated band structures and transmission coefficients. We also show that the width of the band gaps may be enlarged by increasing the strength of the pinning field.

The Green's function method (GFM) used in the calculation in this paper derives a response function which contains all the physical informations of the composite system under study. This response function gives in particular directly the magnetization at any point of the system as response to an unit input excitation introduced at any other point. This method is equivalent to the usual calculation of the eigenvalues and eigenvectors of the composite system by in particular the transfer matrix method [17,18]. Its advantages are in a more compact treatment of the interface boundary conditions and in the fact that this response function enables direct calculations of all the physical properties, in particular of those connected with defects and scattering problems [22]. These Green's functions enable us to obtain analytic expressions for the dispersion relation as well as the reflection and transmission coefficients through the structure. The complete response functions can also be used to derive all eigenvectors [25] in the finite networks.

This study is organized as follows. In Section 2, we deal with infinite and finite CLS. First we use the semi-classical torque equation for the magnetization and the GFM to write down the magnetic GF for an infinite Heisenberg ferromagnetic medium. We then calculate the dispersion relation for CLS and the transmission coefficient. In Section 3, we illustrate these analytical results by numerical examples with emphasis on the effect of the pinning field on the band gap and the transmission spectrum of the networks. Finally, some conclusions are drawn in Section 4.

## 2 Theoretical model

### 2.1 Green's function for an infinite medium

Here we investigate the calculation of the magnetic GF's for an infinite ferromagnetic medium. In using the Heisenberg model of a ferromagnet we are neglecting the

effects of dipole-dipole interactions compared with the exchange contribution to the Hamiltonian. Therefore in evaluating the needed Green's function, it is convenient to use a continuum approximation. Such an approximation is valid provided that the relevant wavelengths are large compared with the lattice spacing. Therefore, we will deal only with long-wavelength excitations.

A medium denoted "$i$" and described in the Cartesian coordinate system ($O$, $x_1$, $x_2$, $x_3$) is assumed to have a simple cubic structure with lattice parameter $a$. We take the static applied field $H_0$ and the spontaneous magnetization $M_0$ to be in the $x_1$ direction. The equation of motion for the total magnetization $\mathbf{M}$ can be expressed in terms of total effective magnetic field $\mathbf{H}$ as

$$\frac{d\mathbf{M}}{dt} = \gamma(\mathbf{M} \times \mathbf{H}) - \Gamma(\mathbf{M} - M_0 i_1), \tag{1}$$

where $\gamma$ is the gyromagnetic ratio and $\Gamma$ is a phenomenological damping factor (considered to be positive constant). The fields $\mathbf{M}$ and $\mathbf{H}$ are given by

$$\mathbf{M} = M_0 i_1 + \mathbf{m}(\mathbf{r}, t), \tag{2}$$

and

$$\mathbf{H} = H_0 i_1 + \mathbf{h}_{ext}(r, t) - \mathbf{H}_{ext} e^{j(\mathbf{k}\cdot\mathbf{r} - \omega t)}. \tag{3}$$

It is understood that $i_1$ is a unit vector parallel to the static fields $M_0$ and $H_0$ in the $x_1$ direction and $\mathbf{m}(\mathbf{r}, t)$ represents the instantaneous deviation from its average value $M_0 i_1$. The term proportional to $\mathbf{H}_{ext}$ in equation (3) represents an externally applied driving field of wave vector $\mathbf{k}$ and frequency $\omega$. Finally the term $\mathbf{h}_{ext}(\mathbf{r}, t)$ in equation (3) is an effective field arising from the exchange interactions between neighboring magnetic moments. This exchange field $\mathbf{h}_{ext}(\mathbf{r}, t)$ may be written as [27]

$$\mathbf{h}_{ext}(\mathbf{r}, t) = \frac{2}{(\gamma\hbar)^2} \sum_{\delta} J_{r,r+\delta} \mathbf{M}(\mathbf{r} + \delta, t), \tag{4}$$

where $J_{r,r+\delta}$ is the exchange interaction between magnetic sites at $\mathbf{r}$ and $\mathbf{r} + \delta$. In this paper we assume that $J_{r,r+\delta}$ couples only nearest neighbors in the simple cubic lattice. On expanding $\mathbf{M}(\mathbf{r} + \delta, t)$ in terms of $\mathbf{M}(\mathbf{r}, t)$ and its derivatives using Taylor series, taking into account that for each site $\mathbf{r}$ there are six neighbors coupled by the exchange $J$, we obtain to the lowest order that,

$$\mathbf{h}_{ext}(\mathbf{r}, t) = \frac{2}{(\gamma\hbar)^2} [6 + a^2 \nabla^2] \mathbf{M}(\mathbf{r}, t). \tag{5}$$

Note that in doing the above expansion we use a continuum representation of the ferromagnet, as was mentioned before, and thus we are restricting ourselves to the long wavelength excitations. Inserting equations (2, 3) and (5) into the torque equation (1), and making the usual linear spin-wave approximation (i.e., neglecting small terms which are of the second order in $\mathbf{m}$, since $|\mathbf{m}| \ll M_0$ at low temperature) we arrive at the following equation of motion for $\mathbf{m}$,

$$\frac{d\mathbf{m}}{dt} + \Gamma\mathbf{m} = i_1 \times \left[\gamma M_0 \mathbf{H}_{ext} e^{j(\mathbf{k}\cdot\mathbf{r} - \omega t)} - \left(\gamma H_0 - D'\nabla^2\right)\mathbf{m}\right], \tag{6}$$

where $D' = 2Ja^2 M_0/\gamma\hbar^2$. From the property of translational invariance of the medium and on assuming a time dependence in the form $\exp[-j\omega t]$, we may write:

$$\mathbf{m}(\mathbf{r}, t) = \mathbf{m}(x_3) e^{j\left(\mathbf{k}_\parallel \cdot \mathbf{x}_\parallel - \omega t\right)}, \tag{7}$$

where $\mathbf{k}_\parallel \equiv (k_1, k_2)$ and $\mathbf{x}_\parallel \equiv (x_1, x_2)$ are two dimensional wave vectors. If we now substitute equation (7) into equations (6), after some algebraic manipulations we arrive at the following differential equation for $m^+(x_3)$,

$$\frac{D'}{\gamma M_0}\left[\frac{\partial^2}{\partial x_3^2} - \mathbf{k}_{||}^2 + \frac{\omega + j\Gamma - \gamma H_0}{D'}\right]\mathbf{m}^+(x_3) = -(H_{ext}^{x_3} + jH_{ext}^{x_2}) e^{jk_3 x_3}, \tag{8}$$

where $m^+(x_3) = m_3(x_3) + jm_2(x_3)$ and $m_1(x_3) = 0$. $k_3$ is the $x_3$ component of the propagation vector $\mathbf{k} = (\mathbf{k}_{||}, k_3)$. Using equation (8), the Fourier-transformed Green's function between two points (sites) $\mathbf{r}(x_1, x_2, x_3)$ and $\mathbf{r}'(x_1', x_2', x_3')$ of the considered infinite ferromagnetic medium "$i$" associated with the magnetization $m^+(x_3)$ satisfies the following equation

$$\frac{F_i}{\alpha_i(\omega)}\left[\frac{\partial^2}{\partial {x_3}^2} - \alpha_i^2(\omega)\right] G_i(k_\parallel, x_3, x_3') = \delta(x_3 - x_3') \tag{9}$$

and can be expressed as

$$G_i(x_3, x_3') = -\frac{e^{-\alpha_i(\omega)|x_3 - x_3'|}}{2F_i} \tag{10}$$

where

$$F_i = \frac{D_i' \alpha_i(\omega)}{\gamma_i M_i}, \tag{11}$$

with

$$\alpha_i(\omega) = \sqrt{k_\parallel^2 - \frac{(\omega - \gamma_i H_0)}{D_i'}}. \tag{12}$$

Let us note that in equation (12) and in what follows the damping constant $\Gamma$ is considered to be zero. The Green's function for a one-dimensional infinite wave-guide is obtained by setting $k_\parallel = 0$ in equation (12), i.e.,

$$\alpha_i(\omega) = j\sqrt{\frac{(\omega - \gamma_i H_0)}{D_i'}}. \tag{13}$$

### 2.2 Interface response theory

We briefly recall the building principle of the Green function of the infinite CLS. This will enable us to present the dispersion relations and the transmitted waves without going into too much detail. Our calculation is based on the theory of interface response in composite materials [25] in which the Green function $g$ of a composite system is given as

$$g(DD) = G(DD) - G(DM)G^{-1}(MM)G(MD) + G(DM)G^{-1}(MM)g(MM)G^{-1}(MM)G(MD) \tag{14}$$

where $D$ and $M$ are the whole space and the space of the interfaces in the composite materials, respectively. $G(DD)$ is the Green's function of a reference continuous medium and $g(MM)$, the interface elements of the Green's function of the composite system. The inverse $g^{-1}(MM)$ of $g(MM)$ is obtained for any point within the space of the interface $M = \{\bigcup M_i\}$ as a superposition of the different $g_i^{-1}(M_i, M_i)$ [25], the inverses of $g_i(M_i, M_i)$ for each constituent $i$ of the composite system.

The interface states can be calculated from [25]

$$\det[g^{-1}(MM)] = 0 \tag{15}$$

showing that, if one is interested in calculating the interface states of a composite, one only needs to know the inverse of the Green's function of each individual block in the space of their respective surfaces and/or interfaces.

Moreover if $U(D)$ [26] represents an eigenvector of the reference system, equation (14) enables the calculation of the eigenvectors $u(D)$ of the composite material

$$u(D) = U(D) - U(M)G^{-1}(MM)G(MD) + U(M)G^{-1}(MM)g(MM)G^{-1}(MM)G(MD). \tag{16}$$

In equation (16), $U(D)$, $U(M)$ and $u(D)$ are row-vectors. Equation (16) provides a description of all the waves reflected and transmitted by the interfaces, as well as the reflection and the transmission coefficients of the composite system. In this case, $U(D)$ must be replaced by a bulk wave launched in one homogeneous piece of the composite material [26].

## 2.3 Dispersion relations and transmission coefficients

Now, we turn to the calculation of spin waves band structures and transmission coefficients for comblike structures using the GFM developed by Dobrzynski [25]. The 1D infinite CLS waveguide can be modelled (see Fig. 1a) as an infinite 1D monomode waveguide (*the backbone*-medium 1, in the direction $x_3$) along which $N'$ side branches of length $d_2$ (medium 2) are grafted at $N$ equidistant sites separated by a length $d_1$, $N$ and $N'$ being integers. The period of the CLS is $d_1$. The interface domain is constituted of all the connection points between the side branches and the backbone. A position (site) along the $x_3$ axis in medium 1 is indicated by $n$, where $n$ is an integer such that $-\infty < n < +\infty$. Here and afterwards the cross-sections of all wires are considered to be much smaller than the considered wavelength, so as to neglect the quantum size effect (or the sub-band structure). Due to the translational periodicity of the system in the direction $x_3$ one can define a wave vector $k_3$ along the axis of the waveguide associated with the period $d_1$. With these ingredients, one can derive analytically the dispersion relation of the CLS, as well as the transmission coefficient through a waveguide containing a finite number of sites.

### 2.3.1 One dimensional infinite comblike structures

The CLS is obtained by coupling together the finite segments of length $d_1$ that constitute the backbone and the finite segments of length $d_2$ composing the side branches. Thus, in the first step, we need to know the surface elements of the Green's function for each finite wire.

For a wire involved in the backbone, both surfaces located at $x_3 = -d_1/2$ and $x_3 = d_1/2$ are free. It is known [25] that for such a case the inverse of the $(2 \times 2)$ matrix $g_1(M_1M_1)$, within the interface space $M_1 \equiv \{-d_1/2, +d_1/2\}$ takes the following form:

$$[g_1(M_1M_1)]^{-1} = \begin{pmatrix} A_1 & B_1 \\ B_1 & A_1 \end{pmatrix} = \begin{pmatrix} g_1^{-1}(-d_1/2, -d_1/2) & g_1^{-1}(-d_1/2, d_1/2) \\ g_1^{-1}(d_1/2, -d_1/2) & g_1^{-1}(d_1/2, d_1/2) \end{pmatrix}, \tag{17}$$

where

$$A_1 = -\frac{F_1 C_1}{S_1}, \tag{18}$$

$$B_1 = \frac{F_1}{S_1}, \tag{19}$$

with

$$C_1 = \cosh[\alpha_1(\omega)d_1], \tag{20}$$

$$S_1 = \sinh[\alpha_1(\omega)d_1]. \tag{21}$$

For a segment constituting a side branch (medium 2), the boundary condition at one extremity of the wire is dependent upon the pinning field $H_A$ that gives rise to a local perturbation $V_A$ in the Hamiltonian such that [22] $V_A = -aH_A/M_2$. With $H_A = 0$, ones recovers the case of a free surface. Thus, $g_2^{-1}(M_2M_2)$ becomes

$$[g_2(M_2M_2)]^{-1} = \begin{pmatrix} A_2 & B_2 \\ B_2 & A_2 + V_A \end{pmatrix}, \tag{22}$$

where $A_2$ and $B_2$ have similar expressions to $A_1$ and $B_1$ with the index 1 replaced by 2.

Within the total interface space of the infinite CLS, the inverse of the matrix giving all the interface elements of the Green's function $g$ is an infinite tridiagonal matrix $[g_\infty(MM)]^{-1}$ [25] formed by linear superposition of the elements $[g_i(MM)]^{-1}$. To find this matrix one has to take into account the respective contributions of media 1 and 2 in the interface domain constituted of all the sites $(n, i, \pm d_1/2)$. To find the contribution of medium 1 to the diagonal elements of the matrix $[g_\infty(MM)]^{-1}$ one has to take the element $g_1^{-1}(-d_1/2, -d_1/2)[= g_1^{-1}(d_1/2, d_1/2)]$ of equation (17) and multiply it by 2 (because at each site we have two pasted segments belonging to medium 1). The contribution of medium 2 to the diagonal elements is obtained by calculating the inverse of the matrix given by equation (22), taking the element $g_2(-d_2/2, -d_2/2)[= g_2(-d_2/2, -d_2/2)]$, finding its reciprocal and multiplying

it by $N'$. Therefore, the matrix $[g_\infty(MM)]^{-1}$ takes the form:

$$[g_\infty(MM)]^{-1} = \begin{pmatrix} 2A_1+W & B_1 & 0 & 0 \\ B_1 & 2A_1+W & B_1 & 0 \\ 0 & B_1 & 2A_1+W & B_1 \\ 0 & 0 & B_1 & 2A_1+W \end{pmatrix}, \quad (23)$$

where

$$W = \frac{N'[V_A A_2 + F_2^2]}{(V_A + A_2)}. \quad (24)$$

Taking advantage of the translational periodicity of the system in the direction $x_3$, the above matrix can be Fourier transformed as

$$[g_\infty(\boldsymbol{k}, MM)]^{-1} = 2A_1 + W + 2B_1\cos(kd_1) \quad (25)$$

where $k$ is the modulus of the 1D reciprocal vector $\boldsymbol{k}$. In the $\boldsymbol{k}$ space, the Green's function of the infinite CLS is obtained by inverting the above equation, i.e.,

$$[g_\infty(\boldsymbol{k}, MM)] = \frac{1}{2A_1 + W + 2B_1\cos(kd_1)}. \quad (26)$$

The dispersion relation of the CLS wave-guide is given by equation (15). A simple algebra leads to the form $\cos(kd_1) = \eta(\omega)$ where

$$\eta(\omega) = C_1 + \frac{N'S_1F_2}{2F_1}\left\{\frac{F_2S_2 - C_2V_A}{F_2C_2 - S_2V_A}\right\}. \quad (27)$$

The above equation for the dispersion relation (after inserting the value of $V_A$ and $F_2$ inside the bracket) takes the form:

$$\eta(\omega) = C_1 + \frac{N'S_1F_2}{2F_1}\left\{\frac{\alpha_2(\omega)aS_2 + C_2\varepsilon}{\alpha_2(\omega)aC_2 + S_2\varepsilon}\right\}, \quad (28)$$

where $\varepsilon = \gamma H_A a^2/D_i'$ is the dimensionless parameter which measures the strength of the pinning field $H_A$ relative to the exchange interaction $J$. If $\varepsilon = 0$ we recover the results of reference [21]. It is straightforward to Fourier analyze back into real space the Green's function $g_\infty(\boldsymbol{k}, MM)$ and obtain:

$$g_\infty(n, n') = \left(\frac{S_1}{F_1}\right)\frac{t^{|n-n'|+1}}{t^2-1}, \quad (29)$$

where the integers $n$ and $n'$ refer to the sites $(-\infty < n, n' < +\infty)$ on the infinite waveguide and the parameter $t$ is given by :

$$t = e^{jkd_1}. \quad (30)$$

### 2.3.2 Transmission coefficient of the finite comblike structures

Finite comb structures are physically realizable rather than infinite ones. Therefore, in this section, we investigate the transmission spectrum of a finite comb. This structure is constructed as follows: a finite piece containing $N$ equidistant side-branches is cut out of the infinite periodic system illustrated in Figure 1a, and this piece is subsequently connected at its extremities to two semi-infinite leading lines. The finite CLS is therefore composed of $N'$ side-branches (medium 2, of length $d_2$) pasted periodically with a finite segment (medium 1) of length $d_1$ at $N$ sites on a finite line. We calculate analytically the transmission coefficient of a bulk spin-wave coming from $x_3 = -\infty$.

The system of Figure 1b is built of the infinite CLS illustrated in Figure 1a. *In a first step*, one suppresses the segment linking sites 0 and 1 as well as the segment linking sites $N$ and $N+1$. For this new system composed of a finite comb and two semi-infinite leads, the inverse Green's function at the interface space, $[g_t(MM)]^{-1}$, is an infinite banded matrix defined in the interface domain of all sites $n$, $-\infty < n < +\infty$. This matrix is similar to the one associated with the infinite CLS. Only a few matrix elements differ, namely, those associated with the sites $n = 0, n = 1, n = N$, and $n = N+1$.

The cleavage operator $V_{cl}(MM) = [g_t(MM)]^{-1} - [g_\infty(MM)]^{-1}$ [25], is the following $4\times 4$ square matrix defined in the interface domain which is constituted of sites $n = 0, n = 1, n = N$, and $n = N+1$

$$V_{cl}(MM) = \begin{pmatrix} -A_1 & -B_1 & 0 & 0 \\ -B_1 & -A_1 & 0 & 0 \\ 0 & 0 & -A_1 & -B_1 \\ 0 & 0 & -B_1 & -A_1 \end{pmatrix}. \quad (31)$$

*In a second step*, two semi-infinite leads (constituted of the same material) are connected to the extremities $n = 1$ and $n = N$ of the finite CLS. With the help of the GFM [25], the perturbing operator $V_p(MM)$(allowing the construction of the system of Figure 1b from the infinite comb) is defined as the $4\times 4$ square matrix [21]

$$V_p(MM) = \begin{pmatrix} -A_1 & -B_1 & 0 & 0 \\ -B_1 & -A_1 - F_1 & 0 & 0 \\ 0 & 0 & -A_1 - F_1 & -B_1 \\ 0 & 0 & -B_1 & -A_1 \end{pmatrix}, \quad (32)$$

where $F_1$ is the inverse surface Green's function of the semi-infinite lead. Using equations (29, 32), one obtains the matrix operator $\triangle(MM) = I(MM) + V_p(MM)g(MM)$ in the space $M$ of sites $n, n' = 0, 1, N, N+1$. For the calculation of the transmission coefficient, we need only the matrix elements $\triangle(1,1)$, $\triangle(1,N)$, $\triangle(N,1)$, and $\triangle(N,N)$, which can be set in the form of the $2\times 2$ matrix $\triangle_s(MM)$:

$$\triangle_s(MM) = \begin{pmatrix} 1+Qt & Qt^N \\ Qt^N & 1+Qt \end{pmatrix} \quad (33)$$

where

$$Q = \frac{t - C_1 + S_1}{t^2 - 1}. \quad (34)$$

The surface Green's function $d_s(MM)$ of the finite CLS in the space of sites 1 and $N$ is given by:

$$d_s(MM) = g_s(MM)[\triangle_s(MM)]^{-1} \tag{35}$$

where

$$g_s(MM) = \frac{tS_1}{F_1(t^2-1)} \begin{pmatrix} 1 & t^{N-1} \\ t^{N-1} & 1 \end{pmatrix} \tag{36}$$

is the matrix constituted of elements of $g(MM)$ associated with sites 1, and $N$. We now calculate the transmission coefficient with a bulk spin-wave coming from, $x_3 = -\infty$, $U(x_3) = e^{-\alpha_1(\omega)x_3}$. Substituting this incident wave in equation (16) and considering equations (10, 35), the transmission coefficient takes the form

$$T = \left| \frac{2S_1(t^2-1)t^N}{(t(C_1-S_1)-1)^2 - t^{2N}(C_1-S_1-t)^2} \right|^2. \tag{37}$$

## 3 Numerical results and discussion

We now illustrate the above analytical results by a few numerical calculations for some specific examples. We report the results of dispersion relations and transmission factors in the 1D CLS. For the sake of simplicity, we have limited ourselves to the case where *identical media* ($F_1 = F_2$) constitute the CLS.

Figure 2 displays the projected band structure of an infinite CLS (Eq. (28)) for given values of $d_1$, $d_2$, $a$, $\varepsilon$ and $D$ such that $d_1 = d_2 = 1500$ Å, $a = 4$ Å, $-0.025 \leq \varepsilon \leq 0.025$ and $D = 1.4 \times 10^{-6}$ Hz respectively [22]. The plot is given as the frequency $\omega - \Omega_0$,($\Omega_0 = \gamma H_0$), (GHz) versus the dimensionless parameter $\varepsilon$. The shaded areas, corresponding to frequencies for which $|\eta| < 1$, represent bulk bands where spin waves are allowed to propagate in the structure. These areas are separated by minigaps where the wave propagation is prohibited. In Figure 2, one can distinguish between two types of minigaps: the gaps created inside the pass-bands due to the existence (strength) of the pinning field, and the gaps, occurring for any value of $\varepsilon$, that are related to the periodicity of the structure and the resonance states of the grafted branches (which play the role of resonators). Two interesting points appear (in the band structure of Fig. 2) with increasing (decreasing) $\varepsilon$ : first, shifting the position of the gaps to a higher (lower) frequencies, second, widening the gaps which created inside the pass-bands due to the existence of the pinning field. Moreover in the negative range of $\varepsilon$ and $\omega - \Omega_0$, there appears a narrow band. This band correspond to the localized surface states at the ends of the resonators. The increase (decrease) in the length $d_2$ of the resonators, makes this band more narrow (wide). This is due to the weak (strong) interaction between these localized states via the backbone (i.e., the more the end of the resonator is far from the backbone, the more the surface states are localized). This also more visible in the negative range of Figure 3 where the length of $d_2$ is shorter than the one given in Figure 2, namely $d_1 = 1500$ Å and $d_2 = 600$ Å,

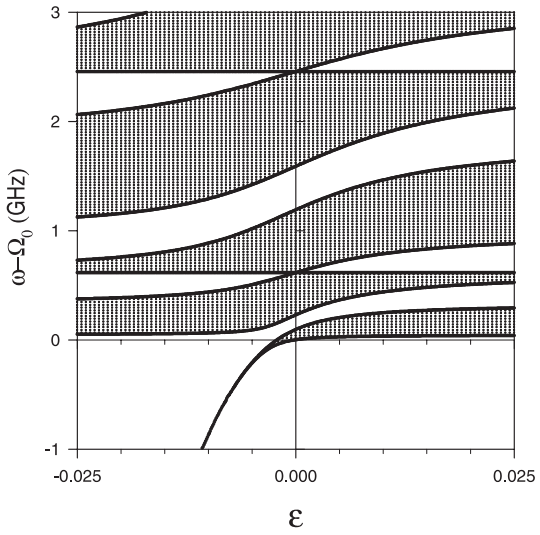


**Fig. 2.** Projected band structure of the CLS as function of $\varepsilon$. The shaded areas represent the bulk bands. The gaps created inside the bulk band is related to the strength of the pinning field. With increasing (decreasing) $\varepsilon$ all gaps are shifted up (down) to a higher (lower) frequencies. The parameters are $d_1 = d_2 = 1500$ Å, $a = 4$ Å, $-0.025 \leq \epsilon \leq 0.025$, $D = 1.4 \times 10^{-6}$ Hz, $N' = 1$, and $N \to \infty$. The two media are identical.

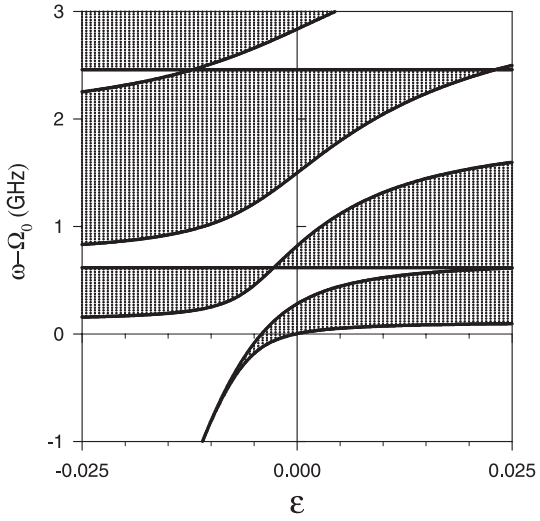


**Fig. 3.** The same as in Figure 2 but for $d_1 = 1500$ Å and $d_2 = 0.4d_1$.

the other parameters being the same as in Figure 2. Let us mention that it is necessary for the existence of the surface (ends) spin waves that $\varepsilon < 0$, i.e. the pinning field $H_A$ is antiparallel to the magnetization direction [22].

As a transparent example we plot in Figure 4 the first five dispersion curves in the band structure of the infinite CLS for two cases, $\varepsilon = 0$ (solid curve) and $\varepsilon = -0.01$ (dashed curve). The plot is given as $\omega - \Omega_0$ (GHz) versus $kd_1$, the other parameters being the same as in Figure 2. The first band for the case $\varepsilon = 0$ disappears with the other choice of $\varepsilon$. A new flat band (which correspond to localized surface states at the ends of the resonators) appear at

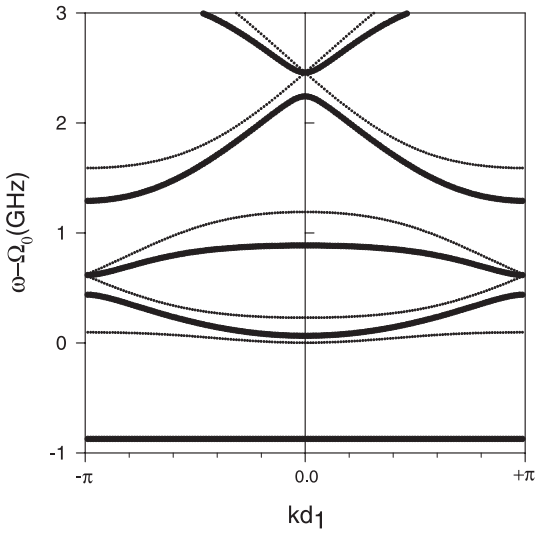


**Fig. 4.** The first five dispersion curves in the spin waves band structure of the infinite CLS for two cases, $\varepsilon = 0$ (dotted curve) and $\varepsilon = 0.01$ (heavy curve). The plot is given as $\omega - \Omega_0$ (GHz) versus $kd_1$. The other parameters being the same as in Figure 2a.

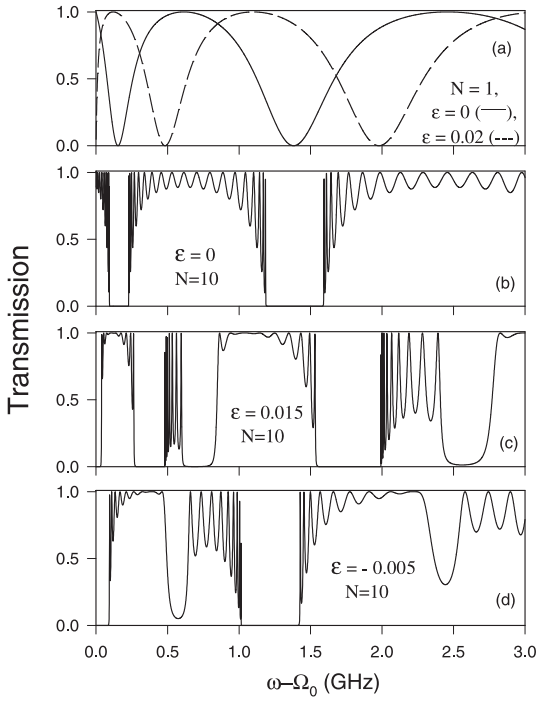


**Fig. 5.** (a) Transmission factor versus frequency (GHz) for a waveguide with one resonator in the case of $\varepsilon = 0$ (solid curve) and $\varepsilon = 0.02$ (dashed curve). The other parameters being as in Figure 2a. (b) Variations of the transmission power through a CLS versus frequency (GHz) for $N = 10$, $N' = 1$ and $\varepsilon = 0$. The other parameters being as in Figure 2a. Figures c, d is the same as in (b) but for $\varepsilon = 0.015, -0.005$ respectively.

$\omega - \Omega_0 \simeq -0.8$ GHz. In the band structure corresponding to $\varepsilon = 0$, the degenerate points between the second and the third bands (which appear at $kd_1 = \pi$ and $-\pi$), and between the fourth and the fifth bands (which appear at $kd_1 = 0$), is removed and a new gaps is created in the band structure corresponding to $\varepsilon = -0.01$. The width, as well as the frequency position, of these gaps depends on the strength of the pinning field.

We now turn to the study of the transmission power through the CLS network (Eq. (37)). We start with a study of a simple example, namely a wave guide consisting of a unique resonator. The variations of $T$ versus frequency, $\omega - \Omega_0$, are reported in Figure 5a for $\varepsilon = 0$ (solid curve) and $\varepsilon = 0.02$ (dashed curve), the other parameters being as in Figure 2. The effect of the pinning field is to shift the zeros of the transmission (which correspond to the eigenmodes of the single resonator) to higher frequencies. These zeros enlarge into gaps with increasing the number of resonators.

The transmission rate through a finite-size of CLS containing $N = 10$ resonators (i.e. $N' = 1$) with $\varepsilon = 0$, 0.015, $-0.005$ is reported in Figures 5b, c and d respectively. New gaps inside the transmission bands show up in these figures. These new gaps are created, firstly, by removing the degenerate points in the band structure (this occurs at small value for $\varepsilon$), see Figure 2. With increasing $\varepsilon$ complete formed gaps are achieved. The position of the gaps related to the periodicity of the structure, as well as the new gaps, shift up to higher frequencies with increasing $\varepsilon$. Despite the finite number of resonators in Figure 5, the transmission approaches zero in regions corresponding to the observed gaps in the spin waves band structure of Figure 2. It is worth noticing that the general features discussed in Figure 2 are still valid for any value of $N$ and $d_1 = d_2$. However, the shape of the band structure changes drastically for $d_1 \neq d_2$, (see Fig. 3).

## 4 Conclusion

In this paper, we have considered the effect of a pinning field on the spin waves band structure and transmission spectra of 1D monomode CLS structures. A theoretical investigation using Green's function method is presented. New gaps are created inside the pass-bands due to the strength of the pinning field. Compared to the study presented in reference [21], the observed gaps can be made larger with special choice of the pinning value. The existence of the gaps in the spectrum is attributed to the periodicity, the zero transmission associated to a single resonator, and the strength of the pinning field. Let us mention that, by associating in tandem several ClS's, one could obtain an ultrawide gap where the transmission is cancelled over a large range of frequencies. In such a structure, the huge gap results from the superposition of the forbidden bands of the individual CLS. Since it is generally the case that magnetic periodic networks have wide technical applications, it is anticipated that this new class of materials, which can be referred to as "spin waves crystals", will turn out to be of significant value for prospective applications.

## References


1. M. Greven, R.J. Birgeneau, U.J. Wiese, Phys. Rev. Lett. **77**, 1865 (1996)
2. S. Chakravarty, Phys. Rev. Lett. **77**, 4446 (1996)
3. D.G. Shelton, A.A. Nersesyan, A.M. Tsvelik, Phys. Rev. B **53**, 8521 (1996); J. Piekarewicz, J.R. Shepard, Phys. Rev. B **57**, 10260 (1998)
4. See, e.g., *The Handbook of Microlithography, Micromachining and Microfabrication*, edited by P. Rai-Chaudhry (SPIE, 1996)
5. R. Arias, D.L. Mills, Phys. Rev. B **63**, 134439 (2001)
6. A. Encinas, M. Demand, L. Piraux, I. Huynen, U. Ebels, Phys. Rev. B **63**, 104415 (2001)
7. J.F. Smyth, S. Schultz, D.R. Fredkin, D.P. Kern, S.A. Rishton, H. Schmid, M. Cali, T.R. Koehler, J. Appl. Phys. **69**, 5262(1991)
8. A. Maeda, M. Kume, T. Ogura, K. Kukoori, T. Yamada, M. Nishikawa, Y. Harada, J. Appl. Phys. **76**, 6667 (1994)
9. N. Bardou, B. Bartenlian, F. Rousseaux, D. Decanini, F. Carcenac, E. Cambril, M.F. Ravet, C. Chappert, P. Veillet, P. Beauvillain, R. Megy, W. Geerts, J. Ferre, J. Magn. Mater. **148**, 293 (1995)
10. A.O. Adeyeye, J.A.C. Bland, C. Daboo, J. Lee, U. Ebels, H. Ahmed, J. Appl. Phys. **79**, 6120 (1996)
11. C. Mathieu, C. Hartmann, M. Bauer, O. Buettner, S. Reidling, B. Ross, S.O. Demokritov, B. Hillebrands, B. Bartenlian, C. Chappert, D. Decanini, F. Rousseaux, E. Cambrill, A. Mueller, B. Hoffmann, U. Hartmann, Appl. Phys. Lett. **70**, 2912 (1997)
12. A. Ercole, A.O. Adeyeye, J.A.C. Bland, D.G. Haskooo, Phys. Rev. B **58**, 345 (1998)
13. J. Jorzick, S.O. Demokritov, C. Mathieu, B. Hillebrands, B. Bartenlian, C. Chappert, F. Rousseaux, A.N. Slavin, Phys. Rev. B **60**, 15194 (1999)
14. D.P. DiVincenzo, D. Loss, Superlattices Microstruct. **23**, 419 (1998); B.E. Kane, Nature (London) **393**, 133 (1998)
15. A.G. Mal'Shukov, K.A. Chao, Phys. Rev. B **61**, R2413 (2000)
16. E.L. Albuquerque, P. Falco, E.F. Sarmento, D.R. Tilley, Solid State Commun. **58**, 41 (1986)
17. M. Krawczyk, J.-C. Lévy, D. Mercier, H. Puszkaski, Phys. Lett. A **282**, 186 (2001)
18. J. Barnas, Phys. Rev. B **45**, 10427 (1992)
19. L.L. Hinchey, D.J. Mills, Phys. Rev. B **33**, 3359 (1986); L.L. Hinchey, D.J. Mills, Phys. Rev. B **34**, 1689 (1986)
20. J.O. Vasseur, L. Dobrzynski, B. Djafari-Rouhani, H. Puszkarski, Phys. Rev. B **54**, 1043 (1996)
21. H. Al Wahsh, A. Akjouj, B. Djafari-Rouhani, J.O. Vasseur, L. Dobrzynski, P.A. Deymier, Phys. Rev. B **59**, 8709 (1999)
22. R.C. Moul, M.G. Cottam, J. Phys. C **12**, 5191 (1979)
23. M.G. Cottam, J. Phys. C **12**, 1709 (1979)
24. C. Kittel, Phys. Rev. **110**, 1295 (1958)
25. L. Dobrzynski, Surf. Sci. Rep. **11**, 139 (1990)
26. L. Dobrzynski, J. Mendialdua, A. Rodriguez, S. Bolibo, M. More, J. Phys. France **50**, 2563 (1989)
27. T.G. Phillips, H.M. Rosenberg, Rep. Prog. Phys. **29**, 285 (1966)